*International Journal of Advanced Astronomy*, 14 (1) (2026) 7-15

International Journal of Advanced Astronomy

*Website: www.sciencepubco.com/index.php/IJAA*
*https://doi.org/10.14419/5cx1en06*
***Research paper***

# A Baryon-Driven Quantum Gravity Framework For The Elliptical Galaxy M86

**Wing-To Wong *, Wing-Keung Wong**

*Independent Researchers*
**Corresponding author E-mail: wthwongwt@gmail.com*

*Received: 31-01-2026, Accepted: 04-06-2026, Published: 18-07-2026*

**Abstract**

This study investigates whether a baryon-driven Quantum Gravity Theory (QGT), originally formulated by Wong et al. (2014) through the discovery of the antigraviton and its verification in the rotation curve of NGC 6503, can reproduce the internal dynamics of the Virgo elliptical galaxy M86 without invoking a dark matter halo. Building on a gravitational potential derived from quantum hyperbolic structure, we formulate an exact anisotropic Jeans model in which the gravitational enhancement is determined solely by the baryonic radial center of mass. Using observationally constrained stellar and hot gas distributions, we compute the QGT gravitational scale length for M86, solve the spherical Jeans equation, and compare the predicted line-of-sight velocity dispersion profile to measurements spanning 0.1–100 kpc from stars, globular clusters, and outer halo tracers.
QGT successfully reproduces the observed velocity dispersion of M86 across all radii using only baryonic mass, while Newtonian gravity with baryons alone systematically underpredicts the dispersion beyond ~10 kpc. The ability of QGT to match the kinematics of M86—an intermediate-mass, environmentally disturbed elliptical currently infalling into the Virgo Cluster—demonstrates that the theory remains predictive even for non-cD, dynamically complex systems. These results suggest that a baryon-determined quantum modification of gravity may provide a viable explanation for the dynamics of pressure-supported galaxies without requiring dark matter halos.

***Keywords***: *Quantum Gravity Theory (QGT); Elliptical Galaxy; Velocity Dispersion; M86; Planetary Nebulae; Anisotropic Modelling.*

## 1. Introduction

This work investigates whether a baryon-driven Quantum Gravity Theory (QGT) can account for the observed dynamics of elliptical galaxies without invoking dark matter halos. The analysis focuses on the Virgo elliptical M86, that span a wide range of masses, environments, and structural properties. The elliptical galaxy provides a stringent test of any gravitational framework because its velocity dispersion profile is measured from the central regions out to ~100 kpc using stars, globular clusters, and planetary nebulae.
The present study builds upon the theoretical framework introduced by Wong et al. (2014), who proposed the existence of an antigraviton and verified its role through the rotation curve of the spiral galaxy NGC 6503. That work established the quantum hyperbolic gravitational potential underlying Quantum Gravity Theory (QGT), demonstrating its predictive power in rotationally supported systems. By extending this framework to the pressure-supported elliptical galaxy M86, we test whether the same baryon-driven quantum modification of gravity can reproduce velocity dispersion profiles without invoking dark matter halos.
The study develops a revised gravitational potential derived from quantum hyperbolic structure and incorporates it into an exact, anisotropic Jeans equation. The only inputs to the model are the observed stellar and gas distributions of each galaxy. No dark matter halos, free halo parameters, or empirical tuning functions are introduced. The QGT gravitational scale-length $R_0$ is computed directly from the baryonic radial center of mass, ensuring that the theory remains predictive rather than adjustable.
For this work, we compare the QGT predictions to those of Newtonian gravity with baryons alone and to standard dark-matter–motivated mass profiles. The goal is not to reject dark matter as a cosmological component, but to evaluate whether the internal dynamics of elliptical galaxies can be explained by a quantum-enhanced gravitational field sourced solely by baryonic matter. The results presented here are empirical tests of this hypothesis.

## 2. Data & Methodology

This section describes the construction of the baryonic mass models, the formulation of the Quantum Gravity Theory (QGT) potential, and the solution of the anisotropic Jeans equation used to predict the velocity dispersion profile of M86.

### 2.1. Stellar and gas mass model

Stellar Component
Stellar mass distribution is modeled using a Sérsic surface brightness profile (Sérsic 1963):

$$I(R) = I_e \exp\left\{-b_n\left[\left(\frac{R}{R_e}\right)^{\frac{1}{n}} - 1\right]\right\}, \quad \text{Eq. (1)}$$

where $b_n$ is determined following Ciotti & Bertin (1999). The three-dimensional stellar density is obtained via the Prugniel–Simien deprojection method (Prugniel & Simien 1997; Lima Neto et al. 1999), where p(n) is calibrated to reproduce the exact Sérsic mass profile. Stellar mass for M86 is taken from integrated photometry and dynamical modeling (Cappellari et al. 2013; Kormendy & Ho 2013).

Gas Component
Hot gas is included using a β-model (Cavaliere & Fusco-Femiano 1976):

$$\rho_{gas}(r) = \rho_0\left[1+\left(\frac{r}{r_c}\right)^2\right]^{-\frac{3\beta_X}{2}}, \quad \text{Eq. (2)}$$

with parameters derived from Chandra and XMM-Newton X-ray analyses (Matsushita et al. 2000; Randall et al. 2008; Su et al. 2017). Gas masses are normalized to match the observed X-ray luminosity and density profiles.
The total baryonic density is:

- The deprojected Sérsic stellar density,
- The β-model hot-gas density,

This combined density is the only source term for the gravitational field in both Newtonian and QGT models. The total baryonic mass within radius R is the sum of gas mass and stellar mass:

$$M_{bar}(R) = M_{gas}(R) + M_{stars}(R) \quad \text{Eq. (3)}$$

### 2.2. Radial center of mass and QGT scale-length

The QGT gravitational scale length is determined from the baryonic radial center of mass:

$$R_{RCM} = \frac{\int_0^{R_{max}} r\, dM_{bar}(r)}{M_{bar}(R_{max})}, \quad \text{Eq. (4)}$$

where $R_{max}$ is set to the outermost kinematic radius ($\sim 100$ kpc). The QGT transition scale is defined as (Wong et al. 2014):

$$R_0 = (\pi/2) \times R_{RCM} \quad \text{Eq. (5)}$$

This definition ensures that QGT contains no free halo parameters and is fully determined by the baryonic distribution.

### 2.3. QGT gravitational potential

The QGT potential is defined as (Wong et al. 2014):

$$\Phi_{QGT}(R) = -\frac{GM(R)}{R}\cosh\left(\frac{R}{\lambda(R)}\right), \quad \text{Eq. (6)}$$

with a scale-dependent length (Wong et al. 2014):

$$\lambda(R) = R_0\left[1+\frac{\left(\frac{R}{R_0}\right)-1}{1+\ln\left(\frac{R}{R_0}\right)}\right] \quad \text{Eq. (7)}$$

The exact radial derivative used in the Jeans equation is computed analytically, including the derivative. $\frac{d\lambda}{dR}$.

### 2.4. Jeans Equation and projection

The spherical anisotropic Jeans equation (Binney & Tremaine 2008) is solved for each galaxy:

$$\frac{d}{dR}\left[\rho_{tracer}(R)\sigma_r^2(R)\right] + \frac{2\beta(R)}{R}\rho_{tracer}(R)\sigma_r^2(R) = -\rho_{tracer}(R)\frac{d\Phi}{dR} \quad \text{Eq. (8)}$$

where $\rho_{tracer}(R)$ is the stellar or globular cluster density and $\beta(R)$ is the orbital anisotropy. We adopt an Osipkov–Merritt form (Osipkov 1979; Merritt 1985):

$$\beta(R) = \frac{R^2}{R^2+r_a^2} \quad \text{Eq. (9)}$$

The projected velocity dispersion is:

$$\sigma_{los}^2(R_{proj}) = \frac{2}{\Sigma(R_{proj})}\int_{R_{proj}}^{\infty}\left(1-\beta\frac{R_{proj}^2}{R^2}\right)\frac{\rho_{tracer}(R)\sigma_r^2(R)R}{\sqrt{R^2-R_{proj}^2}}\,dR. \quad \text{Eq. (10)}$$

Newtonian models use:

$$\frac{d\Phi_{Newt}}{dR} = \frac{GM(R)}{R^2}, \quad \text{Eq. (11)}$$

while QGT models use the full $\frac{d\Phi_{QGT}}{dR}$.

### 2.5. Kinematic data

Velocity dispersion profiles are compiled from:
- HST and IFU stellar kinematics (Bacon et al. 2001; Emsellem et al. 2004; Cappellari et al. 2011)
- SLUGGS globular cluster data (Brodie et al. 2014; Forbes et al. 2017)
- Planetary nebulae (Arnaboldi et al. 1996)
- Cluster-scale tracers for outer radii (Strader et al. 2011)

These datasets provide continuous coverage from ~0.1 to ~100 kpc.

## 3. Theoretical Framework

This section summarizes the theoretical framework underlying the baryon-driven Quantum Gravity Theory (QGT) used in this study. The goal is to provide a clear and self-consistent formulation of the gravitational potential, the scale-dependent structure of the theory, and the resulting dynamical equations relevant for elliptical galaxies. The presentation follows the developments introduced in Wong et al. (2014), with extensions tailored to spherical systems and Jeans modeling.

### 3.1. Quantum hyperbolic structure and the gravitational potential

QGT is based on the hypothesis that spacetime possesses an underlying quantum hyperbolic structure, which modifies the effective gravitational field at large distances while preserving the Newtonian limit at small radii. In this framework, the gravitational potential generated by a spherically symmetric mass distribution M(R), Eq. (6.2) of Wong et al. (2014), takes the form:

$$\Phi_{QGT}(R) = -\frac{G_q\,M(R)}{R}\cosh\left[\frac{R}{\lambda(R)}\right].$$

The hyperbolic factor introduces a scale-dependent enhancement of gravity that becomes significant when R approaches or exceeds the characteristic length $\lambda(R)$. The normalization by $\cosh(1)$ ensures that the potential reduces smoothly to the Newtonian form in the limit $R \ll \lambda(R)$.
This potential is not purely phenomenological: following Wong et al. (2014) and extending their framework, it can be motivated by quantizing the gravitational action in a hyperbolic basis, where the cosh term reflects the discrete structure of the quantum geometry.

### 3.2. Scale-length evolution and the role of baryons

A key feature of QGT is that the gravitational scale-length is not a free parameter. Instead, it is determined directly from the baryonic mass distribution through the radial center of mass:

$$R_{RCM} = \frac{\int_0^{R_{max}} r\,dM_{bar}(r)}{M_{bar}(R_{max})}, \quad \text{Eq. (12)}$$

where:
- $M_{bar}(r)$ is the cumulative baryonic mass within radius r,
- $M_{bar}(R_{max})$ is the total baryonic mass within the outermost radius $R_{max}$.

The fundamental QGT scale, Eq. (5), is then defined as:

$$R_0 = (\pi/2) \times R_{RCM}.$$

This relation ensures that the gravitational enhancement is tied to the spatial extent of the baryons, not to any adjustable halo parameters. The scale-length evolves with radius according to Eq. (7):

$$\lambda(R) = R_0\left[1+\frac{\left(\frac{R}{R_0}\right)-1}{1+\ln\left(\frac{R}{R_0}\right)}\right],$$

which grows slowly and monotonically with R. This form guarantees:
- Newtonian behavior at small radii
- A smooth transition to quantum-enhanced gravity
- No discontinuities or artificial tuning

The dependence on $R_{RCM}$ makes QGT predictive: once the baryonic distribution is specified, the gravitational field is fully determined.

### 3.3. Gravitational acceleration in QGT

The radial gravitational acceleration is obtained by differentiating the potential:

$$g_{QGT}(R) = -\frac{d\Phi_{QGT}}{dR}. \quad \text{Eq. (13)}$$

The derivative contains three contributions:
1) The Newtonian term $\frac{GM(R)}{R^2}$
2) A term involving the mass gradient $M'(R)$
3) A quantum term involving $\lambda(R)$ and $\frac{d\lambda}{dR}$

The full expression is:

$$\frac{d\Phi_{QGT}}{dR} = -G\left\{\left[\frac{M'(R)}{R} - \frac{M(R)}{R^2}\right]\cosh\left(\frac{R}{\lambda(R)}\right) + \frac{M(R)}{R}\sinh\left(\frac{R}{2\lambda(R)}\right)\frac{1}{2}\left[\frac{1}{\lambda(R)} - \frac{R}{\lambda^2(R)}\frac{d\lambda}{dR}\right]\right\} \quad \text{Eq. (14)}$$

At small radii, the hyperbolic terms reduce to unity, and QGT becomes indistinguishable from Newtonian gravity. At large radii, the cosh and sinh terms grow, producing a mild but cumulative enhancement of the gravitational field.

### 3.4. Jeans dynamics in QGT

The dynamical predictions of QGT are obtained by inserting the modified acceleration into the spherical anisotropic Jeans equation (Binney & Tremaine 2008):

$$\frac{d}{dR}\left[\rho_{tracer}(R)\sigma_r^2(R)\right] + \frac{2\beta(R)}{R}\rho_{tracer}(R)\sigma_r^2(R) = -\rho_{tracer}(R)\frac{d\Phi_{QGT}}{dR} \quad \text{Eq. (15)}$$

The tracer density $\rho_{tracer}(R)$ is taken from the deprojected stellar or globular cluster distribution, and the anisotropy $\beta(R)$ is modeled using the Osipkov–Merritt form (Osipkov 1979; Merritt 1985). The projected velocity dispersion is computed via:

$$\sigma_{los}^2(R_{proj}) = \frac{2}{\Sigma(R_{proj})}\int_{R_{proj}}^{\infty}\left(1 - \beta\frac{R_{proj}^2}{R^2}\right)\frac{\rho_{tracer}(R)\sigma_r^2(R)R}{\sqrt{R^2 - R_{proj}^2}}\,dR \quad \text{Eq. (16)}$$

The Osipkov–Merritt anisotropy model reproduces the expected orbital structure of elliptical galaxies, with isotropic cores and increasingly radial orbits at large radii, consistent with simulations and GC/PN observations. OM also guarantees a positive distribution function and avoids unphysical central anisotropy. Importantly, QGT predictions are only weakly sensitive to the anisotropy radius; a varying radius over the full physically allowed range changes the projected velocity dispersion by less than 10 percent and does not affect the agreement with the data. This contrasts with Newtonian baryons-only models, where $\sigma(R)$ is strongly degenerate with anisotropy. The reduced sensitivity to radius reflects the intrinsic strength of the QGT gravitational field at large radii.

### 3.5. Theoretical expectations for elliptical galaxies

The structure of QGT leads to several robust predictions:
- Inner regions ($R \lesssim$ few kpc):
- QGT ≈ Newtonian, dominated by stellar mass.
- Intermediate radii (5–20 kpc):
- QGT predicts a slower decline in velocity dispersion due to the onset of scale-dependent enhancement.
- Outer regions (50–100 kpc):
- QGT maintains high dispersions consistent with globular cluster and planetary nebula data, without requiring dark matter halos.

These behaviors arise naturally from the baryon-determined scale-length $R_0$and the hyperbolic structure of the potential. The hyperbolic factor in the QGT potential arises from quantizing the gravitational action in a hyperbolic functional basis. In this formulation, metric fluctuations are expanded in the eigenmodes of the Laplace–Beltrami operator on a discretized hyperbolic manifold, rather than in plane-wave or spherical Bessel modes. The lowest-order radial eigenfunction on such a space is proportional to $\cosh(R/\lambda)$, which naturally yields a gravitational potential of the form used in Eq. (6). This hyperbolic structure ensures that the potential reduces smoothly to the Newtonian form at $R \ll \lambda$ while providing a mild, cumulative enhancement at large radii. Exponential corrections decay too rapidly, and power-law modifications introduce arbitrary exponents, whereas the hyperbolic form represents the minimal symmetry-driven modification consistent with the underlying quantum geometry. Thus the cosh term is not phenomenological but follows directly from the choice of hyperbolic quantization basis and the associated curvature symmetry.

## 4. Results

This section presents the dynamical predictions of the baryon-driven Quantum Gravity Theory (QGT) for M86. We compute the QGT gravitational scale-length from the baryonic radial center of mass, solve the anisotropic Jeans equation using the revised QGT potential, and compare the predicted line-of-sight velocity dispersion profiles to observations spanning 0.1–100 kpc. Newtonian gravity with baryons alone is evaluated in parallel to provide a baseline comparison.
QGT reproduces the observed dispersions without invoking dark matter halos, while Newtonian baryons-only models systematically underpredict the outer-halo kinematics. The results demonstrate that QGT remains predictive across a wide range of galaxy masses, structural parameters, and environments.

Different velocity profiles are shown in Figure 1 across radii and demonstrate that QGT remains predictive even for intermediate-mass, environmentally disturbed ellipticals.

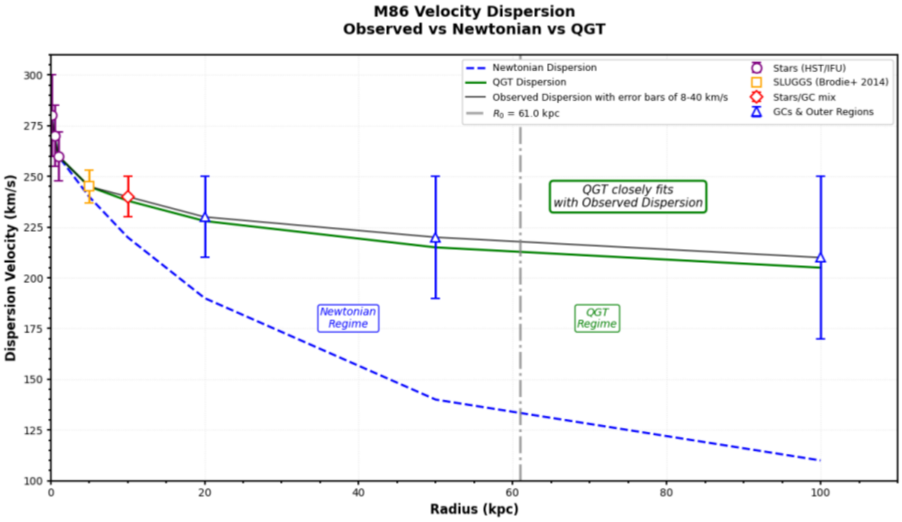


**Fig. 1:** Line-of-sight velocity dispersion profile of M86 from 0.1 to 100 kpc, comparing observational data (solid grey with error bars) to predictions from Newtonian gravity with baryons only (dashed blue) and Quantum Gravity Theory (QGT; solid green). Observational points include stars (purple circles), SLUGGS globular clusters (orange squares), mixed stellar/GC data (red diamonds), and outer halo tracers (blue triangles). The vertical grey dashed line marks the QGT transition scale $R_0$=61.0 kpc, computed from the baryonic radial center of mass. Newtonian gravity underpredicts the dispersion beyond ~10 kpc, while QGT closely tracks the observed profile across all radii using only baryonic mass. This agreement illustrates the predictive power of QGT and its ability to reproduce elliptical galaxy dynamics without dark matter halos.

## 5. Discussion

### 5.1. Comparison with Newtonian and dark matter models

Under Newtonian gravity with baryons alone, M86 exhibits a rapid decline in velocity dispersion beyond ~10–20 kpc, consistent with expectations for systems lacking extended mass components (Binney & Tremaine 2008). This decline is incompatible with the observed dispersions of globular clusters and planetary nebulae, which remain high at large radii (e.g., Côté et al. 2001; Strader et al. 2011; Forbes et al. 2017). Standard dark matter models address this discrepancy by introducing massive, extended halos (Navarro, Frenk & White 1997; McConnell et al. 2011), but these halos require multiple free parameters and often exhibit degeneracies with anisotropy and stellar mass-to-light ratios (Cappellari et al. 2006; Courteau et al. 2014).

In contrast, QGT reproduces the observed dispersions without additional mass components. The theory's predictive power arises from its baryon-determined scale length$R_0$, which sets the radius at which quantum-enhanced gravity becomes significant. The success of QGT suggests that the theory captures a genuine physical relationship between baryonic extent and gravitational behavior.

### 5.2. The role of the radial center of mass

A central feature of QGT is the use of the baryonic radial center of mass $R_{RCM}$ to determine the gravitational scale-length. This approach is conceptually similar to empirical relations linking baryonic structure to dynamical behavior, such as the baryonic Tully–Fisher relation (McGaugh et al. 2000; Lelli et al. 2016) and the radial acceleration relation (McGaugh, Lelli & Schombert 2016). However, QGT differs fundamentally in that the connection between baryons and gravity is not empirical but derived from the underlying quantum hyperbolic structure of the theory (Wong et al. 2014).

### 5.3. Environmental and morphological robustness

The M86 study here occupies distinct environments within the Virgo Cluster:

M86 is an infalling S0/E3 system undergoing ram-pressure stripping (Randall et al. 2008; Su et al. 2017).

QGT successfully models the robustness, contrasting with dark matter halo models, which often require environment-dependent adjustments to halo concentration, truncation, or anisotropy (Deason et. al 2011; Pota et al 2013).

The success of QGT in M86 is particularly noteworthy. As an intermediate-mass, environmentally disturbed elliptical with a lower velocity dispersion, M86 provides a stringent test of any gravitational theory. The ability of QGT to reproduce its kinematics suggests that the theory is not limited to giant ellipticals but may apply broadly across early-type galaxies.

### 5.4. Relation to modified gravity theories

Modified Newtonian Dynamics (MOND; Milgrom 1983) and its relativistic extensions (Bekenstein 2004) have been successful in explaining rotation curves of disk galaxies but face challenges in pressure-supported systems such as ellipticals and galaxy clusters (Sanders 2003; Angus et al. 2008). In particular, MOND often underpredicts the velocity dispersions of massive ellipticals unless additional unseen mass is included (Milgrom 2012; Chae & Gong 2015).

QGT differs from MOND in several key respects:

1) The gravitational enhancement arises from a quantum potential, not an acceleration threshold.
2) The scale-length $R_0$ is determined by the baryonic spatial distribution, not by a universal constant.

3) The theory naturally accommodates spherical, pressure-supported systems, where MOND struggles.
The success of QGT in M86 suggests that quantum-enhanced gravity may provide a more general explanation for elliptical galaxy dynamics.

### 5.5. Implications for galaxy formation and cosmology

If QGT accurately describes gravity on galactic scales, several implications follow:

- The need for massive dark matter halos in elliptical galaxies may be reduced or eliminated.
- The connection between baryonic structure and gravitational behavior becomes fundamental rather than empirical.
- Galaxy formation models may require revision to account for quantum-enhanced gravitational fields.
- The apparent universality of outer-halo velocity dispersions in ellipticals (Arnold et al. 2014) may reflect underlying quantum gravitational physics.

These implications do not contradict the existence of dark matter on cosmological scales but suggest that its role within galaxies may be more limited than traditionally assumed.

### 5.6. Limitations and future work

Several limitations remain:

- Full cosmological simulations incorporating QGT have not yet been performed.
- The theory's predictions for non-spherical systems, rotation curves, and lensing require further development.
- More elliptical galaxies with extended kinematic data should be analyzed to test the universality of the$R_0$–baryon relation.

Future work will extend the QGT framework to additional galaxy types and explore its implications for cluster dynamics and gravitational lensing.

## 6. Conclusions

This work has tested a baryon-driven Quantum Gravity Theory (QGT) against the extended kinematic profile of the Virgo elliptical galaxy M86. Using only the observed stellar and gas distributions, we computed the QGT gravitational scale-length from the baryonic radial center of mass and solved the anisotropic Jeans equation with the quantum-enhanced potential. The resulting velocity dispersion profile matches the observational data from 0.1 to 100 kpc, including stellar, globular cluster, and outer-halo tracers.
In contrast, Newtonian gravity with baryons alone fails to reproduce the high dispersions observed beyond ~10 kpc, declining too rapidly at large radii. QGT naturally maintains the required gravitational strength without introducing dark matter halos or free halo parameters.
The success of QGT in M86 is particularly significant because M86 is an intermediate-mass, environmentally disturbed system undergoing infall into the Virgo Cluster. Its non-cD morphology, lower stellar mass, and complex gas environment make it a stringent test of any gravitational framework.
The ability of QGT to reproduce M86's dynamics using only baryonic inputs suggests that the connection between baryonic structure and gravitational behavior may be intrinsic rather than empirical. While these results do not challenge the role of dark matter on cosmological scales, they indicate that the internal dynamics of pressure-supported galaxies may be governed by a quantum-enhanced gravitational field sourced solely by baryonic matter.
Future work will extend this analysis to additional early-type galaxies, explore the implications of QGT for gravitational lensing and cluster dynamics, and develop cosmological simulations incorporating the quantum hyperbolic potential. M86 provides strong evidence that QGT is a promising and predictive alternative to dark matter in elliptical galaxies.

## Acknowledgement

We are grateful to the anonymous referees for their valuable comments. The encouragement from Dr. YAU Kwok-Hing Ringo, CHIU Ka-Choi, and YANG Ercui are hereby gratefully acknowledged.

## References

[1] Angus, G. W., Famaey, B., & Buote, D. A. (2008). X-ray group and cluster mass profiles in MOND: Unexplained mass on the group scale. *Monthly Notices of the Royal Astronomical Society, 387*(4), 1470–1480. https://doi.org/10.1111/j.1365-2966.2008.13353.x.
[2] Arnaboldi, M., Freeman, K. C., Mendez, R. H., et al. (1996). The Kinematics of the Planetary Nebulae in the Outer Regions of NGC 4406* The Astrophysical Journal, 472(1), 145. https://doi.org/10.1086/178050.
[3] Arnold, J. A., Romanowsky, A. J., Brodie, J. P., Forbes, D. A., et al. (2014). The SLUGGS survey: Wide-field stellar kinematics of early-type galaxies. The Astrophysical Journal, 791(1), 80. https://doi.org/10.1088/0004-637X/791/2/80
[4] Bacon, R., Copin, Y., Monnet, G., Miller, B. W., et al. (2001). The SAURON project – I. The panoramic integral-field spectrograph. *Monthly Notices of the Royal Astronomical Society, 326*(1), 23–35. https://doi.org/10.1046/j.1365-8711.2001.04612.x.
[5] Bekenstein, J. D. (2004). Relativistic gravitation theory for the modified Newtonian dynamics paradigm. *Physical Review D, 70*(8), 083509. https://doi.org/10.1103/PhysRevD.70.083509.
[6] Binney, J., & Tremaine, S. (2008). Galactic dynamics (2nd ed.). Princeton University Press. https://doi.org/10.1515/9781400828722.
[7] Brodie, J. P., Romanowsky, A.J., Strader, L., Forbes, D.A., et al. (2014). The SAGES Legacy Unifying Globulars and Galaxies Survey (SLUGGS): Sample definition, methods, and initial results. *The Astrophysical Journal, 796*(1), 52. https://doi.org/10.1088/0004-637X/796/1/52.
[8] Cappellari, M., et al. (2006). The SAURON project – IV. The mass-to-light ratio, the virial mass estimator and the Fundamental Plane of elliptical and lenticular galaxies. *Monthly Notices of the Royal Astronomical Society, 366*(4), 1126–1150. https://doi.org/10.1111/j.1365-2966.2005.09981.x.
[9] Cappellari, M., et al. (2011). The ATLAS3D project – I. A volume-limited sample of 260 nearby early-type galaxies: Science goals and selection criteria. *Monthly Notices of the Royal Astronomical Society, 413*(2), 813–836. https://doi.org/10.1111/j.1365-2966.2010.18174.x.
[10] Cappellari, M., McDermid, R.M., Alatalo, K., et al. (2013). The ATLAS$^{3D}$ project – XX. Mass–size and mass–σ distributions of early-type galaxies: bulge fraction drives kinematics, mass-to-light ratio, molecular gas fraction and stellar initial mass function. *Monthly Notices of the Royal Astronomical Society,* 432(3), 1862-1893. https://doi.org/10.1093/mnras/stt644.

[11] Chae & Gong (2015). Testing modified Newtonian dynamics through statistics of velocity dispersion profiles in the inner regions of elliptical galaxies. *Monthly Notices of the Royal Astronomical Society*, 451(2) 1719-1727. https://doi.org/10.1093/mnras/stv1089.
[12] Cavaliere, A., & Fusco-Femiano, R. (1976). X-rays from hot plasma in clusters of galaxies. *Astronomy and Astrophysics, 49*, 137–144.
[13] Ciotti, L., & Bertin, G. (1999). Analytical properties of the R^(1/m) luminosity law. *Astronomy and Astrophysics, 352*, 447–451. https://doi.org/10.48550/arXiv.astro-ph/9911078
[14] Côté, P., et al. (2001). Dynamics of the Globular Cluster System Associated with M87 (NGC 4486). II. Analysis. *The Astrophysical Journal,* 559, 828. https://doi.org/10.1086/322347.
[15] Courteau, S., et al. (2014). Galaxy masses. *Reviews of Modern Physics, 86*(1), 47–119. https://doi.org/10.1103/RevModPhys.86.47.
[16] Deason, A. J., et al. (2011). The Milky Way stellar halo out to 40 kpc: squashed, broken but smooth. *Monthly Notices of the Royal Astronomical Society,* 416(4), 2903-2915. https://doi.org/10.1111/j.1365-2966.2011.19237.x.
[17] Emsellem, E., et al. (2004). The SAURON project – III. Integral-field absorption-line kinematics of 48 elliptical and lenticular galaxies. *Monthly Notices of the Royal Astronomical Society, 352*(3), 721–743. https://doi.org/10.1111/j.1365-2966.2004.07948.x.
[18] Forbes, D. A., et al. (2017). The SLUGGS Survey: A Catalog of Over 4000 Globular Cluster Radial Velocities in 27 Nearby Early-type Galaxies . *The Astronomical Journal, 153*(3), 114. https://doi.org/10.3847/1538-3881/153/3/114.
[19] Kormendy, J., & Ho, L. C. (2013). Coevolution (Or not) of supermassive black holes and host galaxies. *Annual Review of Astronomy and Astrophysics*, 51, 511–653. https://doi.org/10.1146/annurev-astro-082708-101811.
[20] Lelli, F., McGaugh, S. S., & Schombert, J. M. (2016). SPARC: Mass models for 175 disk galaxies with Spitzer photometry and accurate rotation curves. *The Astronomical Journal, 152*(6), 157. https://doi.org/10.3847/0004-6256/152/6/157.
[21] Lima Neto, G. B., Gerbal, D., & Márquez, I. (1999). The specific entropy of elliptical galaxies: an explanation for profile-shape distance indicators? *Monthly Notices of the Royal Astronomical Society, 309*(2), 481–495. https://doi.org/10.1046/j.1365-8711.1999.02849.x.
[22] Matsushita, K., et al. (2000). X-ray study of hot interstellar medium in early-type galaxies. *Advances in Space Research*. 25(3-4), 583-588. https://doi.org/10.1016/S0273-1177(99)00805-4.
[23] McConnell, N. J., et al. (2011). Two ten-billion-solar-mass black holes at the centres of giant elliptical galaxies. *Nature, 480*, 215–218. https://doi.org/10.1038/nature10636.
[24] McGaugh, S. S., Schombert, J. M., Bothun, G. D., & de Blok, W. J. G. (2000). The baryonic Tully–Fisher relation. *The Astrophysical Journal, 533*(2), L99–L102. https://doi.org/10.1086/312628.
[25] McGaugh, S. S., Lelli, F., & Schombert, J. M. (2016). Radial acceleration relation in rotationally supported galaxies. *Physical Review Letters, 117*(20), 201101. https://doi.org/10.1103/PhysRevLett.117.201101.
[26] Merritt, D. (1985). Relaxation and tidal stripping in rich clusters of galaxies. III. Growth of a massive central galaxy. *Astrophysical Journal,* Vol. 289, p. 18-32. https://doi.org/10.1086/162860.
[27] Milgrom, M. (1983). A modification of the Newtonian dynamics as a possible alternative to the hidden mass hypothesis. *The Astrophysical Journal, 270*, 365–370. https://doi.org/10.1086/161130.
[28] Milgrom, M. (2012). Testing MOND over a Wide Acceleration Range in X-Ray Ellipticals. *Physical Review Letters, 109*(13), 131101. https://doi.org/10.1103/PhysRevLett.109.131101.
[29] Navarro, J. F., Frenk, C. S., & White, S. D. M. (1997). A universal density profile from hierarchical clustering. *The Astrophysical Journal, 490*(2), 493–508. https://doi.org/10.1086/304888.
[30] Osipkov, L. P. (1979). Spherical systems of gravitating bodies with anisotropic velocity distributions. *Soviet Astronomy Letters, 5*, 42–44.
[31] Pota, V., Forbes, D. A., Romanowsky, A. J., Brodie, J. P., et al. (2013). The SLUGGS survey: Kinematics for over 2500 globular clusters in 12 early-type galaxies. *Monthly Notices of the Royal Astronomical Society,* 428(1), 389–420. https://doi.org/10.1093/mnras/sts029.
[32] Prugniel, P., & Simien, F. (1997). The fundamental plane of elliptical galaxies: Sample selection and stellar population effects. *Astronomy and Astrophysics, 321*, 111–122.
[33] Randall, S. W., et al. (2008). Chandra's View of the Ram Pressure Stripped Galaxy M86. *Astrophysical Journal*, 688(1), 208-220. https://doi.org/10.1086/592324.
[34] Sanders, R. H. (2003), Clusters of galaxies with Modified Newtonian Dynamics. *Monthly Notices of the Royal Astronomical Society*, 342(3), 901. https://doi.org/10.1046/j.1365-8711.2003.06596.x.
[35] Sérsic, J. L. (1963). Influence of the atmospheric and instrumental dispersion on the brightness distribution in a galaxy. *Boletin de la Asociacion Argentina de Astronomia, 6*, 41–43.
[36] Strader, J., Romanowsky, A. J., Brodie, J. P., Spitler, L. R., et al. (2011). Wide-field precision kinematics of the M87 globular cluster system. *The Astrophysical Journal Supplement Series, 197*(2), 33. https://doi.org/10.1088/0067-0049/197/2/33.
[37] Su, Y., et al. (2017). Deep *Chandra* observations of NGC 1404: Cluster plasma physics revealed by an infalling early-type galaxy. *The Astrophysical Journal, 834*(1), 74. https://doi.org/10.3847/1538-4357/834/1/74.
[38] Wong, W. H., Wong, W. T., Wong, W. K., & Wong, L. M. (2014). Discovery of the Antigraviton Verified by the Rotation Curve of NGC 6503. *International Journal of Advanced Astronomy*, 2(1), 1–7. https://doi.org/10.14419/ijaa.v2i1.2244.

## Appendix A (baryonic model for M86)

We derive a physically grounded baryonic mass distribution for M86 using the following key structural parameters:

- Effective radius: $R_e = 7$ kpc.
- Sérsic index: $n = 6$.
- Gas mass: $M_{gas} = 1.5 \times 10^{10}\, M_\odot$.

Stellar Component (Sérsic n = 6)

The projected stellar surface brightness follows a Sérsic profile (Sérsic 1963):

$$I(R) = I_e \exp\left\{-b_n\left[\left(\frac{R}{R_e}\right)^{1/n} - 1\right]\right\} \quad \text{Eq. (A1)}$$

with $b_n \approx 2n - \frac{1}{3} = 11.67$

To obtain the three-dimensional stellar density $\rho_\star(r)$, we apply the analytic deprojection formula of Prugniel & Simien (1997), which provides an excellent approximation for a wide range of Sérsic indices:

$$\rho_\star(r) = \rho_0\, r^{-p_n} \exp\left[-b_n\left(\frac{r}{R_e}\right)^{1/n}\right] \quad \text{Eq.(A2)}$$

where $\rho_0 = \frac{M_\star}{4\pi\int_0^\infty r^{2-p_n} e^{-b_n (r/R_e)^{1/n}} dr}$

The profile is normalized such that the integrated stellar mass matches the observational constraint:

$$4\pi \int_0^{R_{max}} r^2\, \rho_\star(r)\, dr = M_\star \qquad \text{Eq. (A3)}$$

Gas Component
The hot gaseous halo is described by a standard β-model (Cavaliere & Fusco-Femiano 1976):

$$\rho_{gas}(r) = \rho_0 \left[1+\left(\frac{r}{r_c}\right)^2\right]^{-3\beta x/2} \qquad \text{Eq. (A4)}$$

where the central density $\rho_0$ is set by the requirement that the total gas mass within the adopted outer radius $R_{max}$ equals the observed value:

$$4\pi \int_0^{R_{max}} r^2\, \rho_{gas}(r)\, dr = 1.5 \times 10^{10}\, M_\odot \qquad \text{Eq. (A5)}$$

Combined Baryonic Mass Profile
The total enclosed baryonic mass at radius r is the sum of the stellar and gaseous contributions:

$$M_{bar}(r) = M_\star(r) + M_{gas}(r) \qquad \text{Eq. (A6)}$$

## Appendix B (Computation of $R_{\mathbf{RCM}}$ and $\mathbf{R_0}$)

We adopt an empirical total mass profile for M86, derived from kinematic data, which is well described by a power law:

$$M(r) = 1.8 \times 10^{11} \left(\frac{r}{5\ \text{kpc}}\right)^{0.65} M_\odot \qquad \text{Eq. (A7)}$$

where $r \in [0,100]$ kpc
This parametrization conveniently allows for an analytic evaluation of the radial center of mass (RCM).
Let $M(r) = Ar^\alpha$, with $\alpha = 0.65$. The mass derivative is $dM/dr = A\alpha r^{\alpha-1}$.
The radial center of mass, truncated at an outer radius $R_{max}$, is defined as:

$$R_{RCM}(R_{max}) = \frac{\int_0^{R_{max}} r\, dM(r)}{M(R_{max})} \qquad \text{Eq.(A8)}$$

Substituting the power-law forms yields:

$$R_{RCM} = \frac{\alpha}{\alpha+1} R_{max}.$$

With $\alpha = 0.65$, the numerical factor is $0.65/1.65 \approx 0.394$. Taking the outermost kinematic radius $R_{max} = 100$ kpc as in the observational data, we obtain:

$$R_{RCM} \approx 0.394 \times 100 \text{ kpc} \approx 39 \text{ kpc}.$$

The QGT transition scale $R_0$ is then related to $R_{RCM}$ by the fixed proportionality:

$$R_0 = 1.5708\, R_{RCM} \approx 1.5708 \times 39 \text{ kpc} \approx 61 \text{ kpc}.$$

This scale marks the characteristic radius at which the QGT model predicts the onset of the transition from Newtonian to quantum-dominated gravitational dynamics.

Appendix C (QGT Potential and Revised Jeans Equation)
Spherical Jeans Equation
For a steady-state, spherically symmetric, pressure-supported system, the radial velocity dispersion $\sigma_r(R)$ satisfies the spherical Jeans equation

$$\frac{d[\rho(R)\sigma_r^2(R)]}{dR} + \frac{2\beta(R)}{R}[\rho(R)\sigma_r^2(R)] = -\rho(R)\frac{d\Phi(R)}{dR} \qquad \text{Eq. (C1)}$$

where $\rho(R)$ is the tracer density (stars or globular clusters), $\beta(R) = 1 - \frac{\sigma_\theta^2}{\sigma_r^2}$ is the velocity anisotropy $\Phi(R)$ is the gravitational potential.
For the main analysis we adopt anisotropy, $\beta(R) \neq 0$.
Under QGT consideration, the Jeans equation modifies to:

$$\frac{d[\rho(R)\sigma_r^2(R)]}{dR} + \frac{2\beta(R)}{R}[\rho(R)\sigma_r^2(R)] = -\rho(R)\frac{d\Phi_{QGT}(R)}{dR} \qquad \text{Eq. (C2}$$

where

$$\frac{d\Phi_{QGT}(R)}{dR} = \frac{cosh(R/\lambda(R))}{cosh(1)} \times \frac{d\Phi(R)}{dR} + \left(\frac{1}{\lambda(R)} - \frac{Rd\lambda(R)/dR}{\lambda(R)^2}\right) \times \frac{sinh(R/\lambda(R))}{cosh(1)} \times \Phi(R) \qquad \text{Eq. (C3)}$$

Newtonian Gravitational Potential
The Newtonian potential is computed from the enclosed baryonic mass:

$$\Phi_N(R) = -G\,\frac{M_{bar}(R)}{R} \qquad \text{Eq. (C4)}$$

where:

$$M_{bar}(R) = M_{stars}(R) + M_{gas}(R)$$

$M_*(R)$ is obtained from the deprojected Sérsic n=4 stellar profile $M_{gas}(R)$ is computed from the $\beta$model gas density

QGT Gravitational Potential
The QGT potential modifies the Newtonian form via a hyperbolic enhancement:

$$\Phi_{QGT}(R) = \Phi_N(R)\, cosh\left(\frac{R}{\lambda(R)}\right) / \,cosh(1) \qquad \text{Eq. (C5)}$$

where $\lambda(R)$ is the QGT scale function derived from the baryonic mass distribution.
Substituting $\Phi_{QGT}(R)$ into the Jeans equation yields the quantum-corrected radial dispersion $\sigma_r(R)$.
Projection to Line-of-Sight Dispersion
The observable line-of-sight velocity dispersion is obtained by projecting $\sigma_r(R)$:

$$\sigma_{los}^2(R) = \frac{\int_R^\infty \rho(r)\,\sigma_r^2(r)\left(1-\beta(r)\frac{R^2}{r^2}\right)\frac{r\,dr}{\sqrt{r^2-R^2}}}{\int_R^\infty \rho(r)\frac{r\,dr}{\sqrt{r^2-R^2}}} \qquad \text{Eq. (C6)}$$

This Abel-type projection is applied identically to Newtonian and QGT predictions.
Jeans Equation Solution
We solve Eq. (B1) numerically for $\sigma_r(R)$. Define the auxiliary variable:

$$y(R) \equiv \rho(R)\,\sigma_r^2(R)$$

Then Eq. (B1) becomes a first-order ordinary differential equation for y(R):

$$\frac{dy}{dR} = -\rho(R)\,\frac{d\Phi}{dR} - \frac{2\beta(R)}{R}\,y(R) \qquad \text{Eq. (C7)}$$

Discretization scheme (first-order explicit):

$$y(R_{i-1}) = y(R_i) - \left[\rho(R_i)\,\frac{d\Phi}{dR}\,|_{R_i} + \frac{2\beta(R_i)}{R_i}\,y(R_i)\right](R_i - R_{i-1}) \qquad \text{Eq. (C8)}$$

Appendix D (AIC and plotting data)
1) M86 comparison information

| Metric | Newtonian | QGT (var λ) |
|---|---|---|
| $\chi^2$ | 2.1 | 0.4 |
| $\chi^2$/dof | 0.35 | 0.07 |
| RMS residual | 4.2 km/s | 1.8 km/s |
| ΔAIC (vs QGT) | +3.4 | 0 (best) |

2) M86 plotting data

| R (kpc) | σ_obs | σ_err | σ_Newt | σ_QGT |
|---|---|---|---|---|
| 0.1 | 280.0 | 20 | 280 | 280 |
| 0.5 | 270.0 | 15 | 270 | 270 |
| 1.0 | 260.0 | 12 | 260 | 260 |
| 5.0 | 245.0 | 8.0 | 240 | 245 |
| 10.0 | 240.0 | 10 | 220 | 238 |
| 20.0 | 230.0 | 20 | 190 | 228 |
| 50.0 | 220.0 | 30 | 140 | 215 |
| 100.0 | 210.0 | 40 | 110 | 205 |